Hybrid Ferromagnetic-Semiconductor Structures

GARY A. PRINZ

Ultrahigh-vacuum growth techniques are now being used to grow single-crystal films of magnetic materials. These growth procedures, carried out in the same molecular beam epitaxy systems commonly used for the growth of semiconductor films, have yielded a variety of new materials and structures that may prove useful for integrated electronics and integrated optical device applications. Examples are given for growth on GaAs and ZnSe, including magnetic sandwiches and patterned structures.

THE PAST THREE DECADES HAVE WITNESSED THE RAPID advance of solid-state electronics, including first the replacement of discrete circuit elements and finally the integration of many circuit elements onto one semiconductor chip. Schottky barrier diodes replaced rectifier tubes, and various manifestations of the three-terminal transistor replaced the vacuum triode used for signal modulation or amplification. Resistive and capacitive circuit elements were also readily transferred to the new integrated circuit technology. The only fundamental discrete circuit elements that have been left behind in this revolution are those involving magnetic materials. In fact, in all of the dramatic advances made in electronic materials processing over the past decade, very little work has been devoted to incorporating magnetic materials into planar integrated electronic (or photonic) circuitry. This is unfortunate, because there are several tasks for which magnetic materials are irreplaceable, and these uses remain unaddressed in modern integrated electronics. In addition, there are potential applications that have no analog in vacuum electronics but that remain unrealized, awaiting the development of appropriate materials and processing procedures. In this article I will show that ferromagnetic metals can now be prepared in thin-film form compatible with the fabrication of semiconductor devices and that their properties can be exploited for various applications.

Growth of Expitaxial Films

The ferromagnetic metal–semiconductor system that has (Fe/GaAs), been most thoroughly studied is iron/gallium arsenide (Fe/GaAs), although for iron/zinc selenie (Fe/ZnSe) there is now also a large body of data. Both compound semiconductors have the zincblende structure, which is composed of two nested face-centered cubic (fcc) structures, one for each of the constituents. The (unreconstructed) (001) face of the zincblende structure is illustrated in Fig. 1A as viewed in the [001] direction. The projection of the unit cell face is illustrated by the dashed line, and the cubic lattice constant, a_0, is given for both compounds. The sizes of the atoms reflect their ionic radii given on the drawing. Also indicated are the high-symmetry axes in the plane.

These zincblende surfaces support the epitaxial growth of single-crystal Fe films because the size of the unit cell is almost exactly twice that of body-centered cubic (bcc) α-Fe, the low-temperature ferromagnetic phase, as shown in Fig. 1B. In fact, if one pictures an As- or Se-terminated (001) surface, the Fe atoms will occupy the vacant cation sites as well as sites of similar symmetry halfway between any two anion sites along a <100> direction in the (001) plane. A

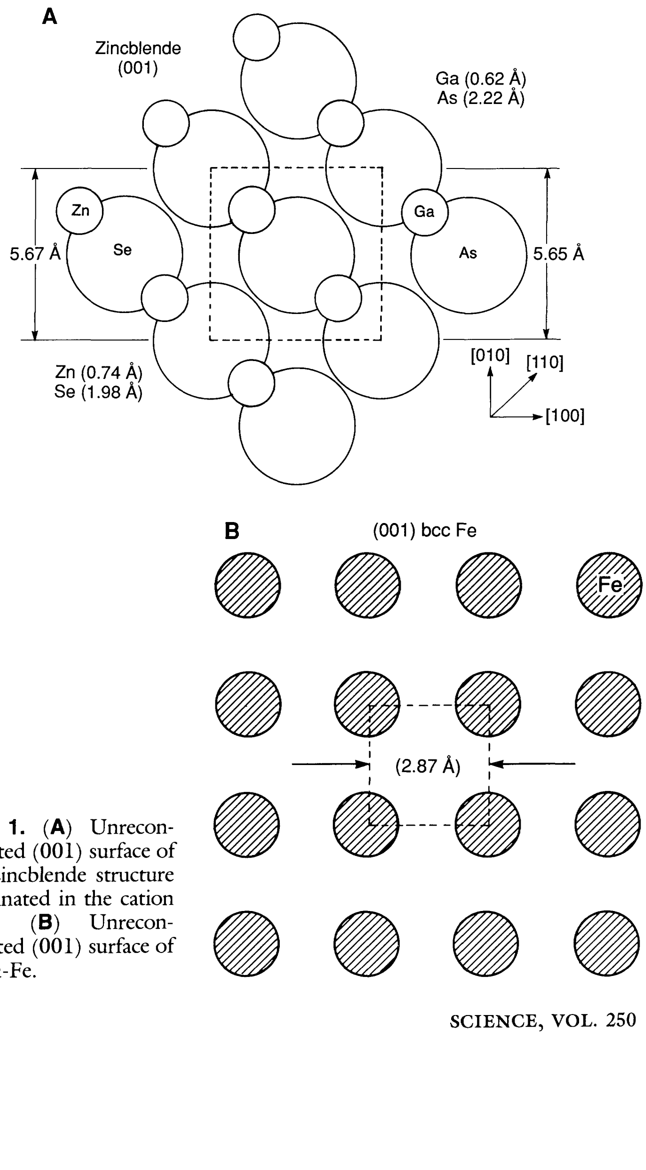

Fig. 1. (**A**) Unreconstructed (001) surface of the zincblende structure terminated in the cation layer. (**B**) Unreconstructed (001) surface of bcc α-Fe.

The author is in the Materials Science and Technology Division, Naval Research Laboratory, Washington, DC 20375.

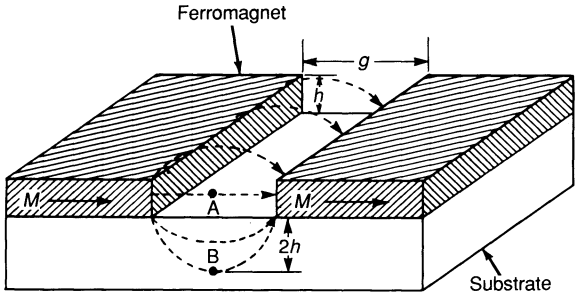

Fig. 2. Magnetic flux generated at the gap in a ferromagnetic film.

pseudomorphic epilayer of Fe arranged in this way is under 1.3% compression on GaAs and 1.0% compression on ZnSe. Because of the factor of 2 size relationship that exists between the two unit cells, oriented parallel epitaxy is obtained as follows,

$$\begin{aligned} (001)_{\mathrm{Fe}} \parallel (001)_{\mathrm{zb}}&:[100]_{\mathrm{Fe}} \parallel [100]_{\mathrm{zb}} \\ (110)_{\mathrm{Fe}} \parallel (110)_{\mathrm{zb}}&:[001]_{\mathrm{Fe}} \parallel [001]_{\mathrm{zb}} \end{aligned} \tag{1}$$

and so on, for all faces, in spite of the fact that the substrate is fcc and the overlayer is bcc. The strain is ultimately relieved by misfit dislocations; however, these are not necessarily generated in the overlayer. Because bcc-Fe is such a stiff structure and so tightly bonded to GaAs, it has been observed in cross-sectional transmission electron microscope photographs that dislocations are actually generated at the interface and penetrate into the GaAs substrate (*1*). The tight bonding is readily observed if one cleaves a GaAs substrate covered with a thick ($\cong 1$ μm) Fe film. The film maintains its integrity, and any attempt to tear it apart at the cleave results in its being peeled off the substrate, tearing small crystallites of GaAs out of the substrate in the process. This bonding is understood from photoemission studies; these studies show the formation of FeAs at the interface, which has a greater heat of formation than GaAs itself. In fact, on the (110) surface of GaAs, which is stoichiometrically balanced, an Fe overlayer actually displaces the surface Ga layers to form FeAs, leaving free Ga metal (*2*).

It is interesting to compare the growth of Fe on III-V GaAs with that on II-VI ZnSe. Although both substrates have zincblende structures and are closely latticed-matched to α-Fe, II-VI compounds are much more ionic and less reactive with Fe than III-V compounds. Consequently, photoemission studies show no evidence of Zn-Fe interchange at the interface. Recent Auger diffraction studies also show that, although Fe exhibits island-like three-dimensional growth at 175°C for low coverages on GaAs, the initial growth of Fe on ZnSe at this temperature proceeds as layer-by-layer two-dimensional growth (*3*). This growth temperature was found to be optimum for Fe/GaAs in terms of the narrowest electron diffraction linewidth. It also correlated well with the optimum magnetic properties such as narrow ferromagnetic resonance linewidth (see below). At lower growth temperatures, there is insufficient energy to anneal the metal surface during growth, resulting in increased step density. Higher temperatures encourage interdiffusion at the Fe/GaAs interface. There is evidence of As leaving the interfacial region and penetrating into the Fe lattice 10 to 20 Å from the Fe/GaAs boundary (*1*), but there is no such evidence for Se near the Fe/ZnSe boundary (*2*).

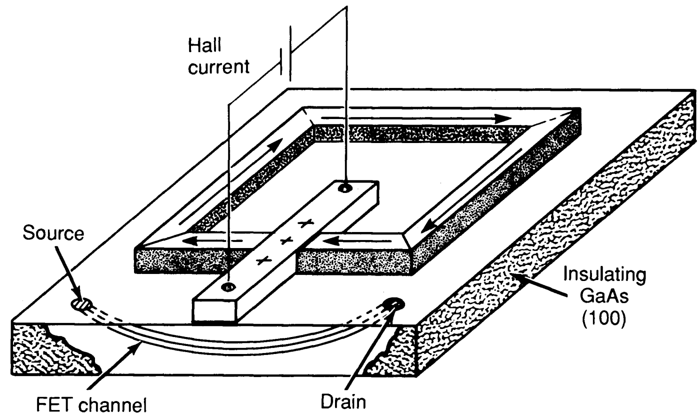

Fig. 4. Thin-film magnetic picture-frame memory element with integrated readout.

These details of the structure, composition, and chemistry near the interface significantly affect the magnetic properties of films several hundred angstroms thick. For certain high-frequency resonance modes they also dramatically alter the electromagnetic boundary conditions at the interface and change the coercive fields (the applied magnetic field necessary to reverse the magnetization). These issues affect various applications of the ferromagnetic films as discussed below.

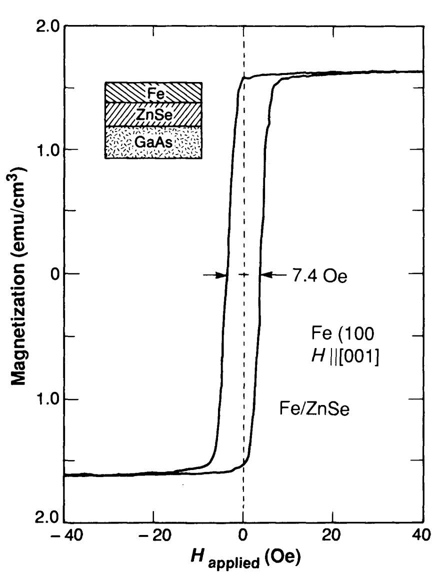

Fig. 3. Hysteresis curve (*M* versus *H*) for Fe film (200 Å) on ZnSe (100). [Adapted from (*8*)]

Magnetostatic Fields

It is well known that the application of magnetic fields to semiconducting materials can produce significant changes in the electrical and optical properties. Indeed, this is one of the most powerful techniques for probing the electronic structure of semiconductors. These properties change because the field either shifts the energy of electronic levels or acts directly on the carriers in the material. However, even though magnetic fields are widely used for studying semiconductors, they are seldom used in device applications because of the difficulty of generating large magnetic fields in device configurations. For example, consider the field that one can generate by simply providing a current-carrying conductor lithographically overlaid in close proximity to some device element. A simple calculation shows that a one-dimensional conductor carrying 1 mA will generate approximately 2 Oe at a point 1 μm away from the conductor axis. This field is too small to be useful, and the significantly higher power levels needed for larger currents would be prohibitive.

However, consider the situation illustrated in Fig. 2. Here we have a ferromagnetic film in which a small gap has been cut. If the magnetization (M) in the film is uniform as indicated, the magnetic poles at the interface will give rise to a magnetostatic field $H = \alpha(4\pi M)$ where $\alpha \geq 1$ and M is magnetization. Two locations are considered: A in the gap and B in the fringing field region. If we assume that the gap width equals the film thickness ($g = h$), then, at A, $\alpha \cong 0.1$. At B (a distance 2 h below the film's bottom surface), $\alpha \cong 0.02$. For Fe, $4\pi M = 21{,}500$ Oe, which gives H 2 kOe at A and $H \cong 400$ Oe at B. These are now fields that may be useful for some purposes, and they are obtained without any dissipative power input into the system. Furthermore, they are fields that are easily manipulated. Figure 3 shows a hysteresis loop (M versus H) for an epitaxial Fe film grown on ZnSe. The coercive field (H_c) is less than 4 Oe. Fields this size are readily obtainable from a current-carrying overlay line. Although the exact magnitude of the static field available and the applied field necessary for rotating it will depend on details of the design of the magnetic circuit, it is this multiplication of 10^2 to 10^3 that encourages one to consider device structures that include magnetic fields to affect performance.

An example of such a proposed device is shown in Fig. 4. It is a magnetic memory element, which is a thin-film analog of a ferrite core. The element is formed by the deposition of an epitaxial magnetic film on a semiconductor substrate, such as Fe on GaAs. Most of the film is lithographically removed except for the square "picture frame" structure shown, which is oriented to have its legs parallel to the [100] axes. These are the magnetically "easy" axes. This structure has only two stable magnetic orientations: it may be magnetized either clockwise (as shown) or counterclockwise. These two states represent either a "0" or "1" bit, respectively. In order to read which bit is set, a small gap is opened in the magnetic circuit as shown and a material is deposited within the gap that exhibits a large Hall effect. By maintaining a current through the Hall bar, a voltage is generated between its upper and lower surfaces, whose polarity reveals the magnetic state of the magnetic circuit. Finally, if the GaAs substrate was prepared, before the deposition of the magnetic and Hall elements, with a source, drain, and channel that lie beneath the Hall bar, then the charge generated on the lower face of the Hall bar can be utilized to bias the field effect transistor (FET) channel beneath it. Thus, in a single compact unit, one has a nonvolatile memory element with semiconductor readout.

Since the magnetic properties are independent of size down to elements of $\cong 10^2$ Å in dimension, the limits of scaling are set by the semiconductor components. Furthermore, since one feature of the picture frame design is that it generates no external magnetic fringing fields, elements can be packed very densely without fear of cross-talk between them. Of course, to complete the device, one must provide overlayer current lines that can carry current pulses of appropriate polarity to reverse the stored bit, but these have not been shown on the figure.

A second device configuration that exploits magnetostatic fields is illustrated in Fig. 5. This also offers a closed magnetic circuit concept; however, it achieves this, not through lithography, but through a sandwich structure. This structure may actually have four stable magnetic states if it is properly constructed. Two of them are shown in Fig. 5, A and B. In the former, the two layers are aligned so that the structure has a net magnetic moment, whereas in the latter they are anti-aligned, forming a closed circuit with no external moment. The other two states are obtained simply by reversing all of the moments in Fig. 2, A and B. This structure has actually been fabricated, and the hysteresis loop is shown in Fig. 5C (*4*).

There are four stable states in zero applied field, not simply the two saturated states shown. The $M = 0$ states are also stable. If one reaches an $M = 0$ condition on the loop and then reduces $H \rightarrow 0$, the system will remain at $M = 0$ in a remnant sate. One might expect from just considering the energy arising from the magnetostatic poles at the edges of the films that only the two $M = 0$ states would be stable. In the absence of magnetic anisotropy, that would be true. However, the two films have different anisotropies because they do not have identical interfaces. One Fe film is grown on GaAs, the other is grown on Ag. This can give rise to different strain or structural anisotropies, which in turn can cause the films to have different coercive fields H_c. The observed behavior in the hysteresis loop arises from the fact that the films reverse at different applied fields, and this effect overwhelms the magnetostatic energy contribution. One may alter the value of these coercive fields at which switching occurs by changing the film thickness and growth conditions. In the absence of anisotropy, the only remaining energy would be the magnetostatic contribution (assuming that there is no coupling through the intervening Ag film). In that case, there would be only two stable states, as with the picture frame, with $M = 0$. Such a structure is in fact utilized in a thin-film magnetic memory element recently reported (*5*). The bits are set by current pulses, but the readout is via the magnetoresistance of the films themselves. The magnetic material in this memory device is Permalloy, and the power requirements are sufficiently low to permit packing densities of 10^8 elements per square centimeter driven by standard CMOS (complementary metal oxide semiconductor) circuitry. Finally, it should be pointed out that, although ferromagnetic coupling through the intervening layer could prevent the $M = 0$ state from being formed, an antiferromagnetic coupling would stabilize it. This has also been recently observed for a very thin Cr layer replacing the Ag intervening layer (*6*).

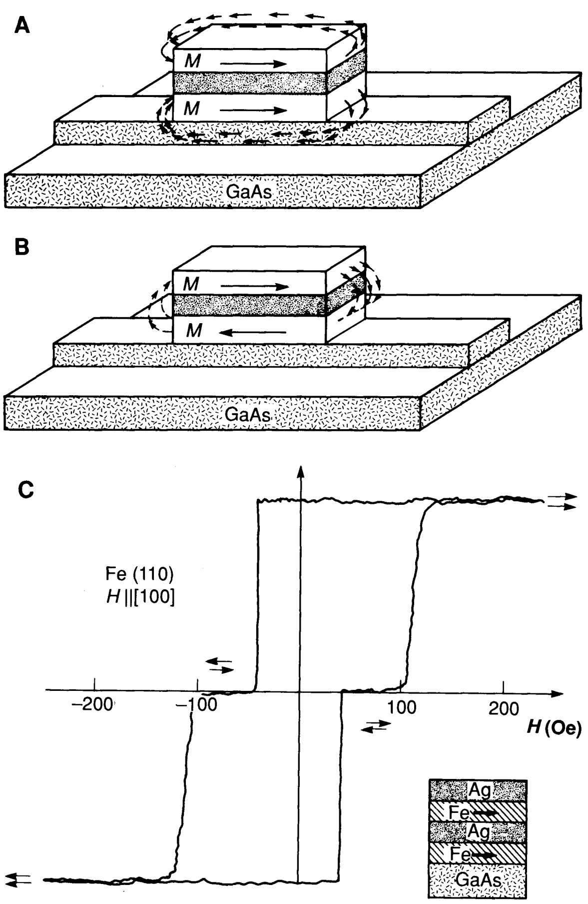

Fig. 5. Magnetic sandwich structure in (**A**) the aligned configuration and (**B**) the anti-aligned configuration. (**C**) Hysteresis curve (M versus H) for the magnetic sandwich structure. [Adapted from (*4*)]

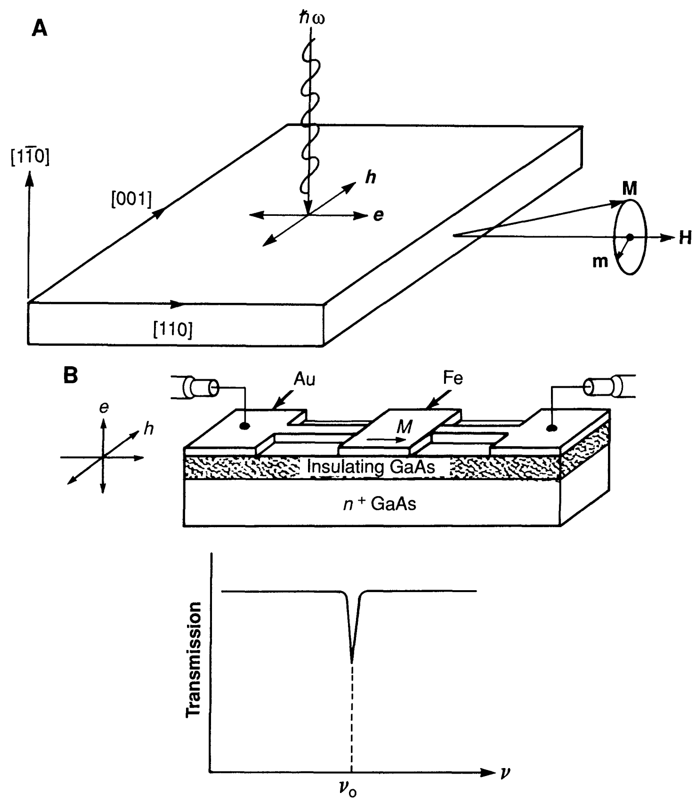

Fig. 6. (**A**) Sketch illustrating plane-polarized radiation of energy $h\tau$ at normal incidence to a film magnetized in the plane ($h\tau$ is Planck's constant). (**B**) Stripline microwave "notch" filter, where ν_0 is defined by Eq. 2.

Coupling to a Radiation Field

One of the most useful properties of magnetic materials is that they can couple to a radiation field. In the microwave region of the spectrum, this coupling occurs when the magnetization vector $\mathbf{M}_0$ is driven by the h component of the radiation. In the most common case with a thin film, the magnetization $\mathbf{M}_0$ lies in the plane of the film. Plane-polarized radiation propagating normal to the plane of the film, as illustrated in Fig. 6A, exerts a torque on the magnetization vector when $h \perp \mathbf{M}_0$, which causes it to exhibit gyroscopic rotation. This system is driven into resonance when

$$2\pi n_0 = \gamma\sqrt{H_{eff}(H_{eff} + 4\pi M_0)} \qquad (2)$$

where ν_0 is the frequency of the radiation, γ is the gyromagnetic ratio, and H_{eff} is the externally applied magnetic field (H_{app}) plus any internal anisotropy field (H_{an}).

For Fe films, where $4\pi M_0$ = 21,500 Oe, this resonance occurs near 10 GHz when $H_{app} = 0$. Here $H_{eff} = H_{an} + H_{app}$ and H_{an} = 500 Oe. This is a very useful frequency regime for many microwave devices. An example is shown in Fig. 6B, which is a schematic drawing of a microwave stripline device concept. Striplines are an effective way to carry microwave signals in planar circuits. They are guided wave devices into which, in this illustration, a microwave signal is injected on the left from a coaxial cable. The n^+ GaAs layer acts as a ground plane, and the structure sustains an electric field between the ground plane and the conducting strip located above the insulating layer of GaAs. The radiation field is thus plane-polarized with its electric vector **e** vertical and the corresponding **h** vector horizontal, and it propagates down the device structure from left to right, emerging on the other end where it is again picked up by another coaxial cable. If a ferromagnetic metal section replaces the conducting strip, as shown, then in that region the radiation field can transfer energy into the ferromagnetic metal if the magnetization vector **M** is parallel to the direction of propagation. In this orientation, the ferromagnetic resonance condition can be satisfied, that is ($\mathbf{M} \perp \mathbf{h}$), and the radiation field can couple to the magnetization. It will, however, couple effectively only at the ferromagnetic resonance frequency $\omega_0 = 2\pi\nu_0$ given above, so that a display of power transmitted versus frequency will show a sharp decrease in transmission at ν_0. This device is called a "notch" filter. The location of the "notch" can be moved by the application of an external magnetic field, as indicated by Eq. 2, parallel to the magnetization direction **M**.

Furthermore, if an external magnetic field is applied perpendicular to the direction **M** as shown in Fig. 6B and has sufficient size to reorient the direction of **M** perpendicular to the direction of signal propagation, the radiation field can then no longer couple to **M**, since now $\mathbf{h} \parallel \mathbf{M}$. This will effectively turn the filter off. As discussed earlier, this requires an H_{app} of <10 Oe, easily achieved in a device configuration. The device described here is intended to be not a prototype design but rather a pedagogical example to illustrate the concepts involved. Real devices are currently under study and have been reported upon (7).

The width of the "notch" in the filter device described is just the linewidth of the ferromagnetic resonance observed in the film. This linewidth is a measure of the quality of the films, insofar as there are variations in **M** or in the internal anisotropy field caused by variations in strain, thickness, or composition. The epitaxial Fe films grown on ZnSe have shown the narrowest linewidths ever observed for a ferromagnetic metal (45 Oe at 35 GHz) (*8*), which become comparable to those observed in ferrimagnetic insulators (ferrites). Ferromagnetic metals were abandoned years ago for high-frequency device applications because their observed linewidths were too large, compared to those of ferrites. These recent results for epitaxial metal films suggest that those conclusions should be reconsidered. This is especially true for higher frequency applications where the low $4\pi M$ of ferrites (≈2 kOe) keeps their zero field resonance frequency low, well below the range of interest for most high-frequency planar device applications.

Spin Injection Devices

One of the most interesting uses of ferromagnetic metal films is as a source of spin-polarized carriers. If one considers the simple Stoner picture of an ideal rigid-band ferromagnetic metal, the majority-spin *d* states lie below the Fermi level and are all filled, but the minority states are filled only up to the Fermi level. Assuming the *s*- and *p*-state electrons to be unpolarized, one might expect that some fraction of the carriers will be polarized to the extent that the minority *d* states contribute to the conductivity. One could exploit this condition to obtain polarized carriers by using a ferromagnetic metal film as an electrical contact on a nonmagnetic metal or semiconductor.

The pioneering work on this concept was reported in 1970 by Meservey *et al.* (*9*), who carried out tunneling experiments from a ferromagnetic metal film through an Al_2O_3 barrier into a superconducting metal film (Al). The superconducting film, with its sharply peaked density of states at the superconducting gap, acted as a spin-polarized electron detector in the presence of an applied magnetic biasing field. The tunneling current, originating from the ferromagnetic film, proved to be highly polarized (+44% for Fe, +34% for Co, and +11% for Ni) (*10*), where the polarization is defined as $P = (n_+ - n_-)/(n_+ + n_-)$, $n_\pm$ being the number of carriers of each spin character.

This was a surprisingly high degree of polarization, but even more surprising was that the polarization direction was that for the majority spins. For the simple band structure assumed, carriers would only be available from the minority spin states near the Fermi level. After several years, an explanation was finally provided by Stearns (*11*), who pointed out that, although most of the *d* electrons occupy energy bands as described by a Stoner model, a small number of *d* electrons have an itinerant character. These itinerant *d* states are the main component of the tunneling current. The relative number of majority and minority spins in these itinerant *d* bands is proportional to the magnetic moment of the material and thus accounts for the observed sign and magnitude of the polarization of the tunneling current.

A more recent achievement in this field was the injection of spin-polarized carriers into a paramagnetic metal by Johnson and Silsbee in 1985 (*12*). This is illustrated in Fig. 7, where the paramagnetic metal (Al) is shown as a long bar with two pads of ferromagnetic metal deposited on it to act as a source and drain of carriers. These carriers will be polarized, since they originate in a magnetized material as shown in the figure. The injected carriers in the first ferromagnetic pad travel through the bar and are picked up at the second ferromagnetic pad. The physics is illustrated, again in a simple Stoner picture, as minority electrons entering the paramagnet, going into unoccupied minority states at the Fermi level; traveling through the metal, under the influence of the applied electric field; and finally, leaving the metal by entering unoccupied minority states in the second ferromagnetic pad. The pads may thus be thought of as polarizing filters acting on the current passing through the circuit.

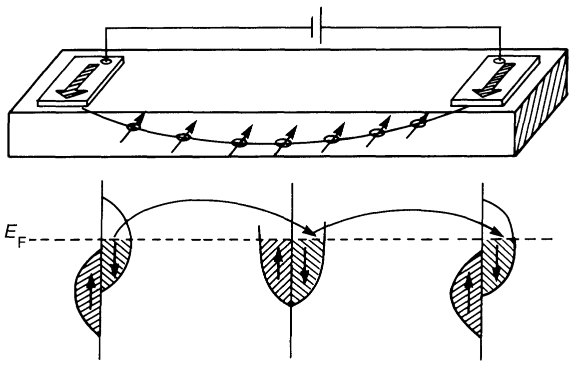

Fig. 7. Injection of spin-polarized current into a paramagnetic bar from ferromagnetic pads. [Adapted from (*13*) with permission of the author]

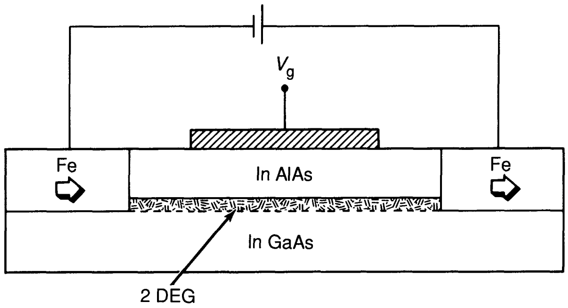

Fig. 8. Proposed spin-polarized FET. 2 DEG, two-dimensional electron gas. [Adapted from (*14*) with permission of the author]

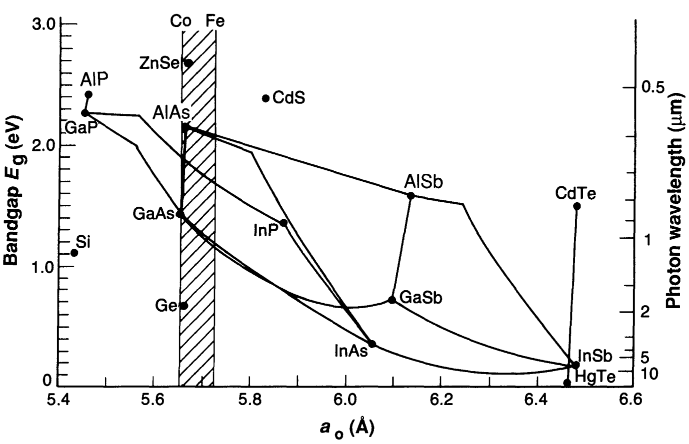

Fig. 9. Lattice constants a_0 of cubic semiconductors with the region of epitaxial lattice match to the bcc Fe-Co alloy system indicated by cross-hatching.

If this picture is correct, the polarized current in the paramagnet should act to unbalance the equally populated up- and down-spin bands, inducing a net magnetization. Because there will be spin-flip scattering events during the transit through the paramagnet, the magnitude of the induced magnetization should decrease along the path. Its measurement would thus yield a determination of the spin-flip scattering length. This measurement was carried out in a system in which thin-film SQUID (superconducting quantum interference device) pick-up loops were put down on the surface of the bar, in a regular array between the two pads, and the induced magnetic moment was measured. It was found that the polarization relaxed with a decay length of 100 µm at 40 K (*13*). It should be noted that, since the two pads act as polarizing filters for the current, if one of them is reversed, the polarized current can be blocked, in much the same way that crossed optical polarizers can block light passing through them.

This analogy was recently invoked for a proposed device that would apply the spin injection concept to ferromagnetic metal films on semiconductors. Datta and Das (*14*) have suggested the construction of a spin-polarized field effect transistor (spin-FET) as illustrated in Fig. 8. The current-carrying medium would be an inversion layer formed at the heterojunction between InAlAs and InGaAs. The two-dimensional electron gas in that layer would provide a very high mobility, free of spin-flip scattering events. The spin-polarized carriers are injected and collected by ferromagnetic metal pads as discussed above. However, one can expect that the strong internal electric field present in the heterostructure interface region in the inversion layer, oriented perpendicular to the layer, will cause the spins of the carriers to precess, as a result of spin-orbit coupling. This precession will rotate them out of alignment with the magnetization of the second ferromagnetic pad, decreasing the transmitted current of the device. Finally, if a gate electrode is deposited on top of the device, one can apply a gate voltage V_g to increase or decrease the effective electric field, causing the spin precession. This will control the alignment of the carriers' spin with respect to the magnetization vector in the second pad, thus permitting modulation of the current passing through the device. Although this proposed device demands carefully controlled material growth and lithography, its fabrication is well within the reach of current technology. Devices such as these, which distinguish between spin-up and spin-down carriers, essentially have an added dimension of device parameters space, which, until now, has not been exploited.

Conclusions

This review provides some examples of the current status of the preparation of hybrid ferromagnetic-semiconductor materials by modern thin-film techniques. The regions of metal-semiconductor epitaxial match are indicated in Fig. 9, with growths already demonstrated for Fe/Ge, Fe/GaAs, Fe/ZnSe, and Co/GaAs. Many of the applications discussed here might be suitable for nonepitaxial magnetic films as well, which opens the way for a host of new possibilities, including alloys of both rare-earth and transition metal ferromagnets, as well as ferromagnetic and ferrimagnetic insulators. Work on these possibilities is under way at a number of laboratories, and it can be anticipated that new hybrid magnetic-semiconducting materials will provide not only technological opportunities but also opportunities for scientifically probing condensed matter behavior.

REFERENCES AND NOTES

1. R. F. C. Farrow *et al.*, in *Epitaxy of Semiconductor Layered Structures*, R. T. Tung, L. R. Dawson, R. L. Gunshor, Eds. (*Mater. Res. Soc. Symp. Proc.* **102**, Pittsburgh, PA, 1988), p. 483.
2. M. W. Ruckman, J. J. Joyce, J. J. Weaver, *Phys. Rev. B* **33**, 1756 (1986).
3. B. T. Jonker and G. A. Prinz, *Bull. Am. Phys. Soc.* **35**, 579 (1990).
4. J. J. Krebs, C. Vittoria, B. T. Jonker, G. A. Prinz, *J. Magn. Magn. Mater.* **54–57**, 811 (1986).
5. A. V. Pohm, J. S. T. Huang, J. M. Daughton, D. R. Krahn, V. Mehra, *IEEE Trans. Magn.* **MAG-24**, 3117 (1988).
6. P. Grunberg, R. Schreiber, Y. Pang, M. B. Brodsky, H. Sowers, *Phys. Rev. Lett.* **57**, 2442 (1986).
7. E. Schloemann, F. Tustison, J. Weissman, H. J. Van Hook, T. Varitimos, *J. Appl. Phys.* **63**, 3140 (1988).
8. G. A. Prinz, B. T. Jonker, J. J. Krebs, J. M. Ferrari, F. Kovanic, *Appl. Phys. Lett.* **48**, 1756 (1986).
9. R. Meservey, P. M. Tedrow, P. Fulde, *Phys. Rev. Lett.* **25**, 1270 (1970).
10. P. M. Tedrow and R. Meservey, *Phys. Rev. B* **7**, 318 (1973).
11. M. B. Stearns, *J. Magn. Magn. Mater.* **5**, 167 (1977).
12. M. Johnson and R. H. Silsbee, *Phys. Rev. Lett.* **55**, 1790 (1985).
13. ———, *Phys. Rev. B* **37**, 5326 (1988).
14. S. Datta and B. Das, *Appl. Phys. Lett.* **56**, 665 (1990).

15. I gratefully acknowledge numerous discussions with many collaborators, in particular J. J. Krebs and K. B. Hathaway. Supported by the Office of Naval Research.

Biomechanics of Mammalian Terrestrial Locomotion

ANDREW A. BIEWENER

Mammalian skeletons experience peak locomotor stresses (force per area) that are 25 to 50% of their failure strength, indicating a safety factor of between two and four. The mechanism by which animals achieve a constant safety factor varies depending on the size of the animal. Over much of their size range (0.1 to 300 kilograms), larger mammals maintain uniform skeletal stress primarily by having a more upright posture, which decreases mass-specific muscle force by increasing muscle mechanical advantage. At greater sizes, increased skeletal allometry and decreased locomotor performance likely maintain stresses constant. At smaller sizes, skeletal stiffness may be more critical than strength. The decrease in mass-specific muscle force in mammals weighing 0.1 to 300 kilogram indicates that peak muscle stresses are also constant and correlates with a decrease in mass-specific energy cost of locomotion. The consistent pattern of locomotor stresses developed in long bones at different speeds and gaits within a species may have important implications for how bones adaptively remodel to changes in stress.

THE INVASION AND EXPLOITATION OF THE EARTH'S TERRESTRIAL environment has yielded a diverse range of animals that share the common problem of movement and support against gravity. This diversity is manifest in size (terrestrial mammals alone span six orders of magnitude in body mass), morphology (shape and number of supporting limbs), locomotor performance, and skeletal materials used. Such diversity raises two important questions: (i) how do animals that differ greatly in size cope with the problem of mechanical support and (ii) do similar mechanical constraints apply to all terrestrial species? Engineering theory can be applied to biological systems to help answer these questions, revealing basic principles that govern locomotor function and the design of skeletal support in living organisms (*1*).

The most important and obvious mechanical requirement for most structures is to avoid breaking. Selection therefore may be expected to favor changes in the form, material organization, or mass of biological structures that decrease the probability of their failure during a lifetime of use. Forces acting on structures, such as those acting on an animal's skeleton during locomotion, are supported as stresses (force per area) developed within the structure. The ratio of failure stress (mechanical strength) to functional stress defines a structure's safety factor (*2*). Failure in a biological sense however need not involve actual rupture of the structure, as excessive deformation (yielding) may render the structure nonfunctional without being ruptured. Although the principle that functional stresses not cause mechanical failure may seem trivial, the question of precisely what safety factor a particular structural element, such as a bone or a tendon, should have (that is, is favored by natural selection) is far less clear, yet critical to an organism's success.

Human-engineered structures commonly are designed to have safety factors ranging from four to ten, depending on the materials of which the structure is built, the cost of the materials, and the accuracy with which the range of forces that the structure is likely to experience can be predicted (*2*). To determine the safety factor of biological structures and whether one safety factor is appropriate for a broad range of species and for different skeletal tissue components, the material properties of skeletal tissues from various species must

The author is an associate professor in the Department of Organismal Biology and Anatomy, University of Chicago, 1025 East 57th Street, Chicago, IL 60637.